International Journal of Nanoelectronics and Materials
IJNeaM
ISSN 1985-5761 | E-ISSN 2232-1535

HTL material variation of Graphene/ITO/TiO_2/$MAPbI_3$/spiro-OMeTAD solar cells under high temperature effect

A. Z. Djennati[a]*, S. Kerai [b], and M. Khaouani [c]

[a] *University Mouloud Mammeri, Tizi-Ouzou 15000, Algeria*
[b] *University Aboubekr Belkaid, Tlemcen 13000, Algeria*
[c] *University of Hassiba Benbouali, Chlef 2000, Algeria*
∗ *Corresponding author. e-mail: abderrahmane-zakarya.djennati@ummto.dz*

Received 2 January 2023, Revised 25 February 2024, Accepted 5 April 2024

ABSTRACT

Perovskite-based solar cells have recently gained attention as a potentially viable option to replace conventional photovoltaic technologies, offering high efficiency and low cost. In this work, we present a numerical simulation of ITO/TiO_2/$MAPbI_3$/OMeTAD solar cell under Silvaco TCAD Tools; the devices exhibit a high efficiency of 27.42 %, 0.3 A/W spectral response at 580 nm optical wavelength. The device is studied under different parameter variations such as: HLT material variation (spiro-OMeTAD, Silicon, PEDOT:PSS and carbon fiber), doping effect of the Sprio layer on IV curves and performance under temperature variation (25-300 ˚C). Overall, this study highlights the potential of perovskite materials in the development of photovoltaic technologies and the accuracy of Silvaco-Atlas in predicting their performance and efficiency.

Keywords: *Perovskite, Solar, Spiro-OMeTAD, Silvaco-Atlas*

1. INTRODUCTION

Organic photovoltaics (OPVs) are attracting attention for their low cost, easy processing and environmental friendliness advantages [1]. Lead amine halide perovskite materials have several advantages for use in solar cells (SC), including: bandgap tunability, efficient light absorption, and high performances [2-6]. The component known as the hole transport layer (HTL) plays a critical role in enhancing the performance of perovskite solar cells (PSC). Its primary function is to transport positive charges, or "holes," from the perovskite light-absorbing layer to the electron transport layer (ETL) and ultimately to the metal electrode. In addition, the HTL plays a role in improving the internal quantum efficiency (IQE) of a device by minimizing charge losses at the interfaces. [7]. The HTL contacted with perovskite layer to extract charge carriers (holes)[8], plays a crucial role on the photovoltaic performance and stability of PSCs. Common HTL materials used in PSCs include spiro-OMeTAD, PCBM (phenyl-C61-butyric acid methyl ester), and PTAA (poly(triarylamine)). The selection of HTL material relies on the specific requirements of the PSCs and can be optimized through experimentation and optimization of the device architecture [9-14]. In just six years from 2009 to 2015, impressive progress has been reported [15,16] using solution-based production methods [10]. The most notable power conversion efficiency (PCE) reported for perovskite solar cells is approximately 25%, as demonstrated in studies [11,17].

This efficiency level is similar to that of traditional solar cells based on silicon.However, ongoing research is aimed at further improving the PCE of perovskite SCs, with the goal of reaching efficiencies above 30% and making them competitive with other technologies for large-scale deployment [18]. The aim of this study is to use Atlas Silvaco TCAD tools to simulate high-efficiency graphene/ITO/TiO_2/$MAPbI_3$/OMeTAD solar cells and study the impact of different HTL materials layer and the temperature effect on the main results of our device.

2. DEVICE DESCRIPTION

The structure of the solar cell is depicted in Figure 1, which shows the proposed configuration of the Graphene/ITO/TiO_2/$MAPbI_3$/OMeTAD solar cell. The device is composed of a transparent graphene contact, an indium tin oxide (ITO) contact, a n-type ETL made of TiO_2, a p-type HTL consisting of spiro-OMeTAD, and an intrinsic perovskite material that serves as the absorber layer. The dimensions of each component are indicated in Figure 1

Table 1 presents a summary of the device's physical parameters that were employed in this work. The parameters are categorized into two parts: band parameters and band-to-band tunneling parameters.

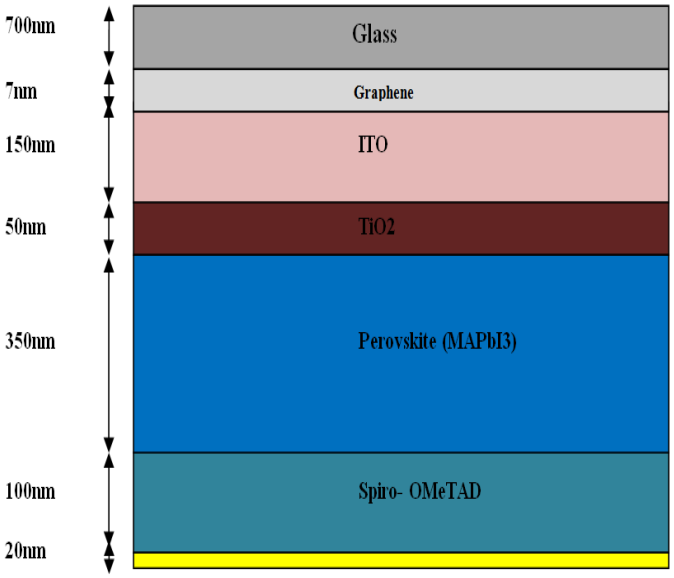

Figure 1 Cross schematic of graphene/ITO/TiO_2/$MAPbI_3$/spiro-OMeTAD solar cells

Table 1 Material parameters

Band parameters	**TiO_2 [30]**	**$MAPbI_3$ [31]**	**HTL OMeTAD**
Epsilon	30	150	3
Eg (eV)	3.2	1.55	3
Chi (eV)	3.9	3.83	2.45
Nc (per cc)	2e+18	1e+019	2e+18
Nv (per cc)	2e+19	1e+17	2e+19
ni (per cc)	8.36e-9	9.56e+4	4e-7
Band-to-band tunneling Parameters			
bb.a	4e+14	4e+14	4e+14
bb.b	1.9e+7	1.9e+7	1.9e+7
bb.gamma	2.5	2.5	2.5
mass.tunnel	0.25	0.25	0.25
me.tunnel	0.185	0.542	0.185
mh.tunnel	0.86	0.0251	0.86

2.1. Models

When using Silvaco Atlas software, a multi-layer stack approach is commonly employed to model perovskite solar cells. This involves creating separate layers for each component of the cell, including the light-absorbing layer, HTL, ETL and metal electrodes. The simulation process entails solving the Poisson and drift-diffusion equations for the charge transport in each layer. Through this approach, important performance metrics, such as photocurrent, open-circuit voltage (VOC), short-circuit current density (Jsc), power conversion efficiency (PCE) and fill factor (FF) can be predicted.

In addition to the device simulation, Silvaco Atlas can also be used to optimize the design of PSCs by varying the parameters of the individual layers, such as the thickness and composition, to find the optimal combination that results in the highest PCE. Recombination of carriers and trapping effects are also defined inside the model by calling Shockley-Read-Hall (SRH) instructions. The output is the Current-Voltage (I-V) plots, where the main performance metrics are extracted [20, 21].

2.2. Methodology

The study commenced with simulations conducted under a standard light power of 1 A/W, spanning a voltage range from -1V to 1V, to comprehensively evaluate the performance of the Graphene/ITO/TiO_2/$MAPbI_3$/OMeTAD solar cell system. First, a graphene layer, precisely 7 nm thick, was integrated into the device structure to augment overall performance.

Subsequently, the investigation delved into variations in the HTL materials, including Spiro-OMeTAD, PEDOT:PSS, silicon, and carbon fiber within a 100 nm thickness. Analysis of the external quantum efficiency (EQE) curves highlighted Spiro-OMeTAD's superior efficiency, prompting further exploration focused on this material. Doping p-type variation analysis within the 100 nm thick Spiro-OMeTAD HTL was conducted across a range from 7e15 cm^{-3} to 2e18 cm^{-3}.

Moreover, the study extended to assess the photovoltaic cell's response to varying temperatures, ranging from 25 to 300 degrees Celsius also based on spiro-OMETAD, simulating real-world operating conditions. This comprehensive investigation aimed to elucidate the interplay of material composition, doping concentration, and temperature effects on device performance. The electrical parameters used in these simulations are detailed in Table 2.

Table 2 Electrical parameters of different HTL material

	Spiro-OMeTAD	**PEDOT: PSS**	**Silicon**	**Carbon fiber**
Eg300 (eV)	3	1.57	1.12	0.9
Affinity (eV)	2.45	3.6	4.05	1.25
Nc300 (cm^{-3})	2e+18	2e+21	2.8e+19	2.8e+19
Nv300 (cm^{-3})	2e+19	2e+21	1.04e+19	1.04e+19
Epsilon	3	3.1	11.9	10

3. RESULTS AND DISCUSSION

3.1. I-V Performance Characterization

The I-V curve shown in Figure 2 of the Graphene/ITO/TiO_2/$MAPbI_3$/OMeTAD solar cell illustrates 27.42% efficiency, along with appropriate values of the VOC and FF.

This high efficiency is attributed primarily to the effects of interfacial traps, as well as the series resistance (R_S) and the shunt resistance (R_{SH}).

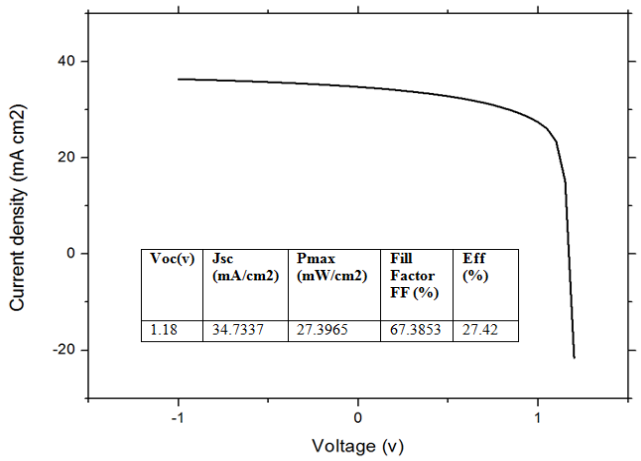

Figure 2 I-V curve for the graphene/ITO/TiO_2/$MAPbI_3$/spiro-OMeTAD solar cells

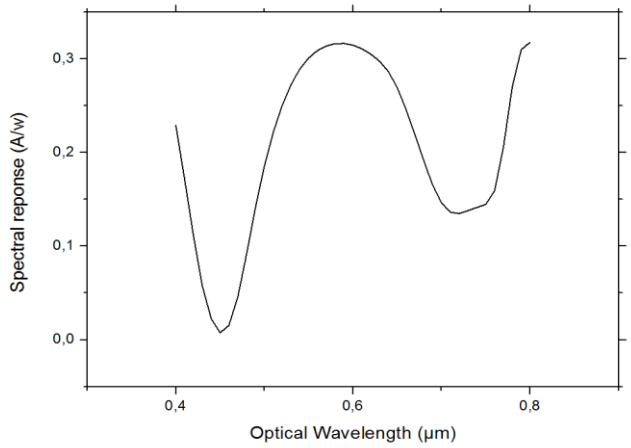

Figure 3 Spectral response curves for the graphene/ITO/TiO_2/ $MAPbI_3$/spiro-OMeTAD solar cells

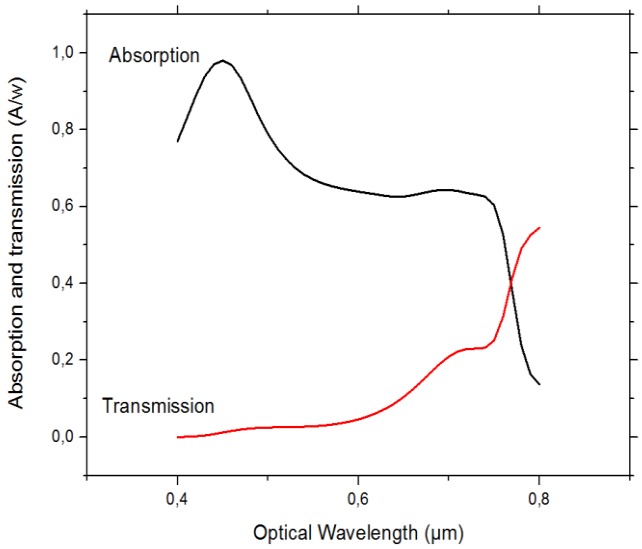

Figure 4 Transmission and absorption curves for the graphene/ITO/TiO_2/$MAPbI_3$/spiro-OMeTAD solar cells

The spectral response is a measure of the cell's ability to convert different wavelengths of light into electrical energy. It is an important performance metric as it provides insight into the cell's light harvesting efficiency and the potential for optimizing the cell's design. It also defines the relative short-circuit current versus the wavelength. Figure 3 depicts the spectral response as a function optical wavelength of graphene/ITO/TiO_2/ $MAPbI_3$/OMeTAD solar cell, showing a 0.3 A/W spectral response at 580 nm optical wavelength.

Based on the above theory, the curves of absorption and transmission as a function of optical wavelength are crucial. They describe at which high or precise optical wavelength values the absorption is most significant, contributing to a high collection of light. The substantial 90% absorption at 450 nm, as shown in Figure 4, highlights the efficient utilization of incident light, further emphasizing the significance of the chosen material configuration.

3.2. External Quantum Efficiency Based on Different HTL Material

The EQE is a parameter used to gauge the capacity of a solar cell to convert incoming photons into electrical current. It is expressed as a percentage and determined by calculating the ratio of electrons gathered at the electrodes to incident photons [22]. The expected variation in the results is mainly due to the different used materials and vertical structure for each type of cell [23]. A study on mono-crystalline silicon solar cells at 350-1100 nm wavelength, was conducted by Chander et al. [24]. It shows that EQE increased from 350 nm wavelength until reaching extreme value at 590 nm, followed by a slow decrease to 970 nm, next to a rapid decrease to the wavelength value of 1100 nm [23,25]. The measurement EQE is achieved in hybrid organic-inorganic third-generation solar cell. In perovskite solar cells, the most common method of measuring EQE involves exposing the cell with single wavelength light and then measuring the photocurrent as a function of the wavelength. The EQE of PSC is generally high, due to the broad absorption spectrum of perovskite materials and the efficient charge transport properties of the materials [26]. Figure 5 shows the EQE curve as a function of optical wavelength using various HTL material.

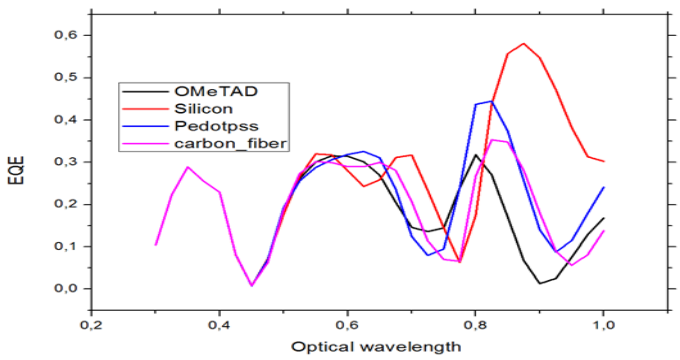

Figure 5 EQE curves with various HTL materials

The curve closely resembles the experimental data reported in [32], providing validation for our simulation model. The intrinsic parameters, behavior under stressing, degradation pathways, and doping schemes of HTL are important characteristics that researchers in various fields can utilize. These properties are specifically relevant to the devices that use spiro-OMeTAD as organic semiconductors [27-29]. In PSCs, the HTL layer plays a vital role as the hole-transporting material (HTM). Its primary function is to transport holes from the perovskite layer to the ETL, where they can be collected as electrical current. Therefore, the quality and stability of the HTM are crucial for the overall performance and efficiency of the PSCs. In Table 3, we present the impact of varying HTL materials on the primary parameters of Graphene/ITO/TiO_2/ $MAPbI_3$/OMeTAD solar cells. It can be observed that Spiro-OMeTAD demonstrates favorable characteristics, exhibiting a significant 15% increase in the value of efficiency compared to silicon. This underscores the widespread adoption of Spiro-OMeTAD as the HTM due to its high hole mobility, thermal stability, and compatibility with perovskite materials.

Table 3 Effect of HTL materials variation

	Spiro-OMeTAD	PEDOT:PSS	Silicon	Carbon fiber
Voc(V)	1.17	1.03	1	1
Jsc (mA/cm2)	34.77	37.90	37.62	35.39
FF(%)	67.39	64.16	62.92	62.96
PCE(%)	27.42	25.13	23.79	22.35
Pmax (mW/cm2)	27.43	25.14	23.80	22.35

3.3. External Quantum Efficiency Based on Different HTL Material

The influence of doping the HTL in PSCs may have a non-negligible impact on the cell's performances. Positive doping can increase the carrier mobility and reduce the recombination of charge carriers, leading to improved charge transport and higher photovoltaic performance. On the other hand, excessive doping or using an inappropriate doping material can lead to reduce absorption of light and lower efficiency. In general, optimal doping of the HTL is crucial for optimizing the performance of PSCs.

Figure 6 demonstrates the influence of doping in HTL with different concentration values (5e17, 1e18, and 2e18 atom/cm^{-3}). The extracted results in Table 4 reveal a 24% increase in efficiency between the lowest (5e17 cm^{-3}) and highest (2e18) doping values. This emphasizes the role of doping concentration in optimizing the charge transport properties within the solar cell.

The efficiency of PSCs can be influenced by temperature, with an increase in temperature often leading to an efficiency deterioration. This reduction in efficiency is primarily due to the adverse effect that higher temperatures have on the stability of the structure of perovskite. High temperatures can also cause degradation of the perovskite layer and the electrodes, leading to decreased performance and lifetime.

Figure 7 illustrates the impact of temperature variation on the performance parameters, such as PCE, Jsc, FF, and VOC of Graphene/ITO/TiO2/MAPbI3/OMeTAD solar cells. The figure demonstrates that changes in temperature can lead to a shift in the bandgap, resulting in a modification of the absorption spectrum of the material. Specifically, as the temperature rises, the bandgap of the perovskite material may reduce, causing an increase in the absorption of light with longer wavelengths and a decrease in the efficiency.

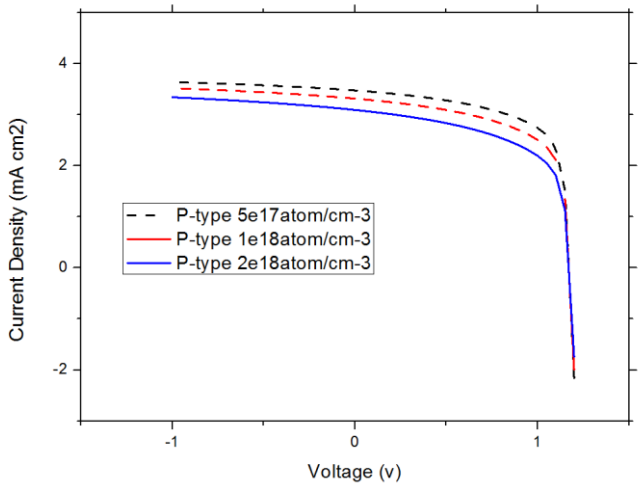

Figure 6 Effect of HTL doping on I-V curves for the graphene/ITO/TiO_2/$MAPbI_3$/spiro-OMeTAD

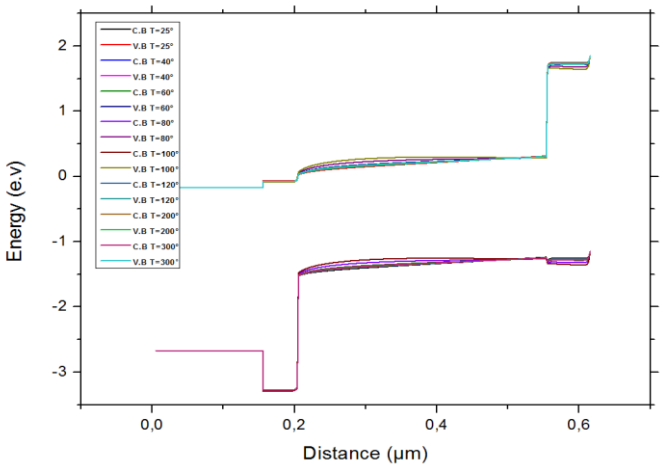

Figure 7 Band diagram curves (VB: valence band, CB: conduction band) for the graphene/ITO/TiO_2/$MAPbI_3$/spiro-OMeTAD solar cell

Table 5 presents the impact of temperature variation on the performances. At high temperatures, the perovskite material can start to degrade, leading to a drop in the efficiency of 4.5% for a temperature variation between 25 °C and 100 °C. In addition, high temperatures can also cause an increase in the resistance of the electrodes and interconnections, reducing the flow of current and further decreasing the efficiency.

These simulation results are pivotal for advancing experimental studies in several ways. They provide a predictive framework for understanding the impact of various parameters, guiding researchers in optimizing material composition, HTL selection, and doping strategies

before embarking on resource-intensive experimental efforts. The simulation outcomes serve as a roadmap, allowing for targeted and efficient experimental designs, reducing trial-and-error iterations. Additionally, Table 6 has been included to present the efficiency of perovskite solar cells from different works alongside our study.

Table 4 Effect of HTL doping variation

Doping value	Voc (V)	Jsc (mA/cm2)	FF (%)	PCE (%)	Pmax (mW/cm²)
5e17	1.16	30.95	60.81	21.96	21.97
1e18	1.17	33.17	64.60	25.07	25.08
2e18	1.17	34.77	67.39	27.42	27.43

Table 5 Effect of temperature variation

Temperature	Voc (V)	Jsc (mA/cm2)	FF (%)	PCE (%)	Pmax (mW/cm²)
25°	1.17	34.77	67.39	27.42	27.43
40°	1.15	34.47	66.85	26.63	26.64
60°	1.12	34.02	66.14	25.32	25.33
80°	1.10	33.57	65.31	24.17	24.18
100°	1.06	33.13	64.96	22.99	23.07
120°	1.05	33.12	64.90	22.88	23.03
200°	0.92	30.93	61.93	17.72	17.72
300°	0.77	28.72	58.82	13.12	13.13

Table 6 Efficiency comparison of different PSCs

PSC	ETL	HTL	PCE (%)
[33]	TiO_2	NiO	23.8
[34]	TiO_2	Sprio-OMETAD	27.0
[34]	PCBM	PEDOT:PSS	24.0
[35]	TiO_2	Sprio-OMETAD	19.5
This work	TiO_2	Sprio-OMETAD	27.43

4. CONCLUSION

In conclusion, the investigation into the Graphene /ITO/TiO_2/$MAPbI_3$/OMeTAD solar cell system has yielded valuable insights into the intricate interplay of various parameters influencing its performance. The exemplary 27.42% efficiency demonstrated in the I-V curve underscores the considerable potential of this configuration for high-performance solar energy conversion. The spectral response at 580 nm and the remarkable 90% absorption at 450 nm emphasize the device's efficiency in harnessing solar radiation across a broad spectrum, crucial for real-world applications. The examination of different HTL materials highlights Spiro-OMeTAD as a promising candidate, showcasing superior efficiency compared to conventional silicon. This emphasizes the pivotal role of HTL material selection in achieving optimal solar cell performance. Further exploration of doping effects in the HTL reveals a nuanced relationship between doping concentration and efficiency, with a notable 15% increase observed between the lowest and highest doping values.

REFERENCES

[1] K. A. Mazzio and C. K. Luscombe, "The future of organic photovoltaics," J. Chem. Soc., vol. 44, no. 90, 2014.

[2] O. Malinkiewicz et al., "Perovskite solar cells employing organic charge-transport layers," Nature Photon., vol. 8, pp. 128-132, 2014.

[3] J. Jeng et al., "Nickel oxide electrode interlayer in $CH_3NH_3PbI_3$ perovskite/PCBM planar-heterojunction hybrid solar cells," Adv. Mater., vol. 26, pp. 4107-4113, 2014.

[4] K. Y. Lou et al., "Seed-mediated superior organometal halide films by GeO_2 nano-particles for high-performance perovskite solar cells," Appl. Phys. Lett., vol. 108, 053301, 2016.

[5] Z. Menga, "Investigation of Al_2O_3 and ZrO_2 spacer layers for fully printable and hole-conductor-free mesoscopic perovskite solar cells," Appl. Surf. Sci.,

[6] Z. Li, J. Zhang, Y. Xu, M. Xue, H. Wang, J. Duan, and H. Wang, "Improving photovoltaic performance of perovskite solar cells: The interfacial modification

role of aluminum chloride and ammonia on ZnO nanorods," *Funct. Mater. Lett.*, vol. 10, 1750017, 2017.

[7] W. Tress, N. Marinova, O. Inganäs, M. K. Nazeeruddin, S. M. Zakeeruddin, and M. Grätzel, "The role of the hole-transport layer in perovskite solar cells - reducing recombination and increasing absorption," in *2014 40th PVSC*, p. 1563.

[8] W. Yang, B. Park, E. Jung, N. Jeon, Y. Kim, D. Lee, S. Shin, J. Seo, E. Kim, J. Noh, and S. Seok, "Iodide management in formamidinium-lead-halide-based perovskite layers for efficient solar cells," *Science*, vol. 356, pp. 1376-1379, 2017.

[9] Z. Wang and L. Liao, "Doped Charge-Transporting Layers in Planar Perovskite Solar Cells," *Adv. Optical Mater.*, vol. 6, 1800276, 2018.

[10] M. Li, Z. Wang, Y. Yang, Y. Hu, S. Feng, J. Wang, X. Gao, and L. Liao, "Copper Salts Doped Spiro-OMeTAD for High-Performance Perovskite Solar Cells," *Adv. Energy Mater.*, vol. 6, 1601156, 2017.

[11] J. Wang, Z. Wang, M. Li, C. Zhang, L. Jiang, K. Hu, Q. Ye, and L. Liao, "Doped Copper Phthalocyanine via an Aqueous Solution Process for Normal and Inverted Perovskite Solar Cells," *Adv. Energy Mater.*, vol. 8, 1701688, 2018.

[12] S. Ameen, M. Rub, S. Kosa, K. Alamry, M. Akhtar, H. Seo, H. Shin, A. Asiri, and M. Nazeeruddin, "Perovskite Solar Cells: Influence of Hole Transporting Materials on Power Conversion Efficiency," *ChemSusChem*, vol. 9, pp. 10-27, 2016.

[13] Y. Hou, X. Du, S. Scheiner, D. McMeekin, Z. Wang, N. Li, M. Killian, H. Chen, M. Richter, I. Levchuk, N. Schrenker, E. Spiecker, T. Stubhan, N. Luechinger, A. Hirsch, P. Schmuki, H. Steinruck, R. Fink, M. Halik, H. Snaith, and C. Brabec, "A generic interface to reduce the efficiency-stability-cost gap of perovskite solar cells," *Science*, vol. 358, pp. 1192, 2017.

[14] A. Marchioro, J. Teuscher, D. Friedrich, M. Kunst, R. van de Krol, T. Moehl, and M. Grätzel, "Ultrasmooth organic-inorganic perovskite thin-film formation and crystallization for efficient planar heterojunction solar cells," *Nat. Commun.*, 2015.

[15] G. Hodes, "Perovskite-Based Solar Cells," *Science*, vol. 342, pp. 317, 2013.

[16] M. A. Green, K. Emery, Y. Hishikawa, W. Warta, and E. D. Dunlop, "Solar cell efficiency tables (version 46)," *Prog. Photovoltaics*, vol. 23, pp. 805, 2015.

[17] A. Kojima, K. Teshima, Y. Shirai, and T. Miyasaka, "Organometal Halide Perovskites as Visible-Light Sensitizers for Photovoltaic Cells," *J. Am. Chem. Soc.*, 2009, 131, 6050.

[18] R. Dunbar, B. Duck, T. Moriarty, K. F. Anderson, N. Duffy, C. Fell, J. Kim, A. Ho-baillie, D. Vak, Y. Wu, K. Weber, A. R. Pascoe, Y.-B. Cheng, Q. Lin, P. Burn, R. Bhattacharjee, H. Wang, and G. Wilson, "How reliable are efficiency measurements of perovskite solar cells? The first inter-comparison, between two accredited and eight nonaccredited laboratories," J. Mater. Chem. A, 2017.

[19] R. C. I. MacKenzie, Gpvdm manual, 2016.

[20] R. C. I. MacKenzie, T. Kirchartz, G. F. A. Dibb, and J. Nelson, "Modeling nongeminate recombination in P3HT: PCBM solar cells," J. Phys. Chem. C, vol. 115, pp. 9806-9813, 2011.

[21] J. Nelson, The Physics of Solar Cells, London, UK: Imperial College Press, 2003.

[22] J. Metzdorf, "Calibration of solar cells. 1: The differential spectral responsivity method," Appl. Opt., vol. 26, no. 9, pp. 1701–1708, 1987.

[23] S. Chander, A. Purohit, A. Nehra, S. P. Nehra, and M. S. Dhaka, "A Study on Spectral Response and External Quantum Efficiency of Monocrystalline Silicon Solar Cell," Int. J. Renew. Energy Res., vol. 5, no. 1, pp. 1–4, 2015.

[24] A. A. Ennaouia, M. Lux-Steinera, et al., "Cu2ZnSnS4 thin film solar cells from electroplated precursors: Novel low-cost perspective," Thin Solid Films, vol. 517, no. 7, pp. 2511–2514, 2009.

[25] C. Goh, S. R. Scully, and M. D. McGehee, "Effects of molecular interface modification in hybrid organic-inorganic photovoltaic cells," J. Appl. Phys., vol. 101, no. 11, 2007.

[26] U. Bach, D. Lupo, P. Comte, et al., "Solid-state dye-sensitized mesoporous TiO2 solar cells with high photon-to-electron conversion efficiencies," Nature, vol. 395, pp. 583–585, 1998.

[27] J. Burschka, N. Pellet, S. J. Moon, et al., "Sequential deposition as a route to high-performance perovskite-sensitized solar cells," Nature, vol. 499, pp. 316–319, 2013.

[28] Z. Xiao, Q. Dong, C. Bi, Y. Shao, Y. Yuan, and J. Huang, "Solvent Annealing of Perovskite-Induced Crystal Growth for Photovoltaic-Device Efficiency Enhancement," Adv. Mater., vol. 26, pp. 6503-6509, 2014.

[29] B. Liu, X. Zhao, J. Yu, I. P. Parkin, A. Fujishima, and K. Nakata, "Intrinsic intermediate gap states of TiO2 materials and their roles in charge carrier kinetics," J. Photochem. Photobiol. C, vol. 39, pp. 1-57, 2019.

[30] X. Yang, F. Lv, Y. Yao, P. Li, B. Wu, C. Xu, and G. Zhou, "Boosting Performance of Inverted Perovskite Solar Cells by Diluting Hole Transport Layer," Nanomaterials, vol. 12, no. 22, 2022.

[31] I. Montoya De Los Santos, H. J. Cortina-Marrero, M. A. Ruíz-Sánchez, L. Hechavarría-Difur, F. J. Sánchez-Rodríguez, M. Courel, and H. Hu, "Optimization of CH3NH3PbI3 perovskite solar cells: A theoretical and experimental study," Solar Energy, vol. 199, pp. 198-205, 2020.

[32] R. Itten and M. Stucki, "Highly Efficient 3rd Generation Multi-Junction Solar Cells Using Silicon Heterojunction and Perovskite Tandem: Prospective Life Cycle Environmental Impacts," *Energies*, vol. 10, pp. 841, 2017.

[33] M. Monteiro Lunardi, A. Wing Yi Ho-Baillie, J. P. Alvarez-Gaitan, S. Moore, and R. Corkish, "A life cycle assessment of perovskite/silicon tandem solar cells," *Prog. Photovolt: Res. Appl.*, vol. 25, pp. 679–695, 2017.

[34] I. Celik, A. B. Phillips, Z. Song, Y. Yan, R. J. Ellingson, M. J. Heben, and D. Apul, "Energy Environ. Sci.", vol. 10, 1874, 201